Doping and temperature dependence of nuclear spin relaxation in *n*-type GaAs

L. Abaspour, P. Sterin, E. P. Rugeramigabo, J. Hübner,* and M. Oestreich†
Institute for Solid State Physics, Appelstrße 2, Leibniz Universität Hannover, 30167 Hannover, Germany

(Received 1 July 2020; revised 18 September 2020; accepted 24 November 2020; published 21 December 2020)

We investigate the strong field nuclear spin relaxation rate in *n*-type GaAs for doping densities from the quasi-insulating over the metal-to-insulator up to the quasimetallic regime. The rate measured at 6.5 K increases in the quasi-insulating regime with doping density due to nuclear spin diffusion to the donor electrons and shows a distinct maximum at the critical density of the Mott metal-to-insulator transition. The density dependence of the nuclear spin relaxation rate can be quantitatively calculated over the whole density regime taking into account the effective number of localized electrons and the interaction of free electrons via the Korringa mechanism. Only the nuclear spin relaxation rate of the very lowest doped sample shows a significant deviation from these calculations. Temperature-dependent measurements suggest in this case an additional nuclear spin relaxation channel which is negligible at higher doping densities and is linked to the electron spin relaxation time.

DOI: 10.1103/PhysRevB.102.235205

I. INTRODUCTION

Nuclear spin relaxation (NSR) in *n*-doped GaAs is strongly influenced by the presence of donor electrons [1–8]. Especially localized donor electrons interact at low temperatures very efficiently via hyperfine contact interaction with the nuclear spin system. The resulting NSR times are only fractions of a second for nuclei which are located within the Bohr radius a_B of a localized donor electron [9]. The spin relaxation of remote nuclei is at finite external magnetic fields typically orders of magnitude slower since the spin diffusion toward these relaxation centers is rather slow. The NSR rate due to diffusion, Γ_D, can be approximated for low donor densities, n_d, and zero temperature by [10]

$$\Gamma_D \approx 4\pi D_{\mathrm{av}} n_d a_B. \tag{1}$$

Paget [1] estimated with this approximation from optically detected nuclear magnetic resonance measurements in high purity GaAs an average nuclear spin diffusion coefficient for the three isotopes of $D_{\mathrm{av}} \approx 10^{-13}\ \mathrm{cm}^2/\mathrm{s}$.

Equation (1) describes the typical bulk NSR rate Γ only for n_d well below the metal-to-insulator transition (MIT) and for temperatures where ionization of the localized donor electrons can be neglected. At high temperatures and doping densities above the MIT the donor electrons are delocalized and thereby transformed from very efficient local relaxation centers to a Fermi gas which interacts by electron spin fluctuations with the nuclear spins. This interaction is described in the case of free electrons in the conduction band via the Korringa mechanism and yields a bulk NSR rate

$$\Gamma_K = \frac{\pi}{\hbar} A_{\mathrm{HF}}^2 v_0^2 \rho^2(E_F) k_B T, \tag{2}$$

where $A_{\mathrm{HF}} = \frac{\mu_0}{4\pi}\frac{8\pi}{3}\gamma_e\gamma_n\hbar^2 \cong 44\ \mu\mathrm{eV}$ is the average hyperfine (HF) interaction constant, v_0 is the volume of the primitive unit cell, $\rho(E_F)$ is the density of states at the Fermi energy E_F, and γ_e and γ_n are the gyromagnetic ratios of electron and nuclei, respectively [11–15]. Nuclear spin relaxation in the region of the MIT at finite temperatures is slightly more complex since the localization of the donor electrons changes with increasing n_d due to the overlap of the electron wave functions and the resulting coexistence of strongly localized electrons, weakly interacting donor electrons, the occurrence of impurity bands, and the occupancy of the conduction band.

The combination of both major NSR mechanisms, (a) localized electrons acting as efficient spin relaxation centers in conjunction with nuclear spin diffusion and (b) free electrons as the source for the Korringa mechanism yields a good qualitative picture of the NSR in *n*-doped GaAs at external magnetic fields higher than the local magnetic field B_L [16]. The so called local magnetic field results from the magnetic interaction within the nuclei spin system and is in GaAs less than 2 mT. We will focus in the following on the NSR in external magnetic fields with $B_L \ll B \ll 100$ mT, where the influence of B_L on the NSR as well as magnetic field induced spin polarization of the donor electrons can be neglected. The main goal is to study to which extend the unpretentious picture outlined above describes NSR in the doping regime from quasilocalized to quasifree electrons *quantitatively*.

The doping dependence of the NSR in *n*-GaAs has been studied in the region of the MIT before. Recently, detailed photoluminescence (PL), Faraday rotation, and spin noise measurements on bulk and various microstructured GaAs samples were carried out in Ref. [16]; however, surprisingly no significant variation has been observed in the whole regime from quasilocalized to quasifree electrons of the high field ($B \gg B_L$) NSR rate. We have therefore chosen for the following studies a *contiguous* set of well-characterized, high-quality samples, which have been extensively studied by magnetotransport and Hanle experiments concerning their

*Corresponding author: jhuebner@nano.uni-hannover.de
†Corresponding author: oest@nano.uni-hannover.de

TABLE I. Experimentally determined doping densities n_d^{exp} of the investigated GaAs samples. See Ref. [17] for further details on the equally named samples and the respective temperature-dependent Hall measurements.

Sample no.	S1	S3	S4	S5	S7	S8	S9	S10
n_d^{exp} (10^{16} cm^{-3})	0.120(3)	0.658(9)	0.895(6)	1.732(7)	4.02(9)	6.02(8)	8.20(5)	10.31(5)

electrical, optical, and electron spin relaxation properties and thus allow highly comparable measurements.

II. SAMPLES AND EXPERIMENTAL SETUP

All measurements are performed on quasi-identical, *n*-doped, 2-μm-thick GaAs:Si epilayers grown by molecular beam epitaxy with nominal doping densities ranging from $n_d = 1.2 \times 10^{15}$ to 1.03×10^{17} cm^{-3}, enclosed by specially adapted *n*-doped top and bottom layers in order to reduce surface and interface effects due to depletion. The doping regime covers the whole regime from strongly localized carriers up to the fully degenerate case (Table I). A gives a short overview of the sample parameters while Ref. [17] summarizes for all samples *in extenso* doping density, detailed parameters concerning the impurity band, hopping and/or momentum relaxation rates at 6.5 K, the electron spin relaxation rates, and, around the MIT, the ionized impurity scattering angles.

The nuclear spin relaxation rate is measured following the well-established temporal scheme of (a) optical nuclear spin initialization; (b) NSR in the dark, i.e., without optical excitation; and (c) measurement of the remaining nuclear spin polarization by a Hanle-like polarization measurement of the PL. The technique is described in detail in Ref. [16] and references therein and utilizes the shift of the Hanle curve in the presence of nuclear spin polarization. The samples are placed for the experiments in a microcryostat, cooled to 6.5 K if not stated otherwise, and excited repetitively for time periods of 300 s above band gap by circularly polarized laser light with a photon energy of 1.58 eV and an intensity as low as 0.2 W cm^{-2} at the sample surface. An 800-nm short-pass filter ensures that no residual light from the laser diode compromises the PL detection. A magnetic field B_{pump} is applied during optical excitation by an electromagnet in nearly Voigt geometry ($\approx 10^\circ$ deviation from the Voigt axis). After the dynamic polarization of the nuclear spins, the laser excitation is switched off by a mechanical shutter for a variable dark time t_{dark} during which the optically induced nuclear spin polarization, which is directly related to an effective nuclear magnetic field B_N, relaxes. The external magnetic field is switched during this dark time to B_{dark}. After t_{dark}, the shutter is opened again, the magnetic field is switched to B_{pump}, and the degree of circular polarization of the PL is measured time-resolved in reflection geometry by a 50-kHz photoelastic modulator, a linear polarizer, an 800-nm long-pass filter, a photodiode, and a lock-in amplifier. The high-quality longpass filter is used to efficiently block laser reflections. In principle, the degree of circular polarization directly after opening the shutter, ρ_{dark}, is already a good indirect measure of B_N after t_{dark}. However, measuring the temporal change of the PL polarization during optical excitation and extrapolating this transient to the time where the shutter is opened increases the measurement accuracy of ρ_{dark} and accordingly of the effective B_N. In practice, the nearly Voigt geometry allows to combine the optical pumping of the nuclear spin ensemble and the measurements of the remaining nuclear spin polarization from the previous pump process into one step (see Appendix A for further experimental details and the extraction of B_N from ρ_{dark}).

The NSR rate is measured by repeating the above measurement protocol for different t_{dark}. The inset in Fig. 1 shows exemplary the measured B_N in dependence on t_{dark} for $n_d = 1.73 \times 10^{16}$ cm^{-3} and $B_{\text{dark}} = 2.344(44)$ mT. The solid blue line is an exponential fit which yields an NSR rate $\Gamma = 0.005\,50(21)$ Hz [18]. The whole procedure is then repeated for varying B_{dark} which yields the magnetic field dependence of Γ as depicted in Fig. 1 for $n_d = 1.73 \times 10^{16}$ cm^{-3}. The NSR rate follows the Lorentzian like function [19]

$$\Gamma(B_{\text{dark}}) = \Gamma_Z \frac{B_{\text{dark}}^2 + \xi\, B_L^2}{B_{\text{dark}}^2 + B_L^2}, \tag{3}$$

where $\xi = \Gamma_{ss}/\Gamma_Z$ with Γ_{ss} and Γ_Z being the spin relaxation rates originating from the spin-spin and the Zeeman interaction term, respectively. The ratio ξ is a fitting parameter and weights the heat capacities due to spin-spin coupling and due to Zeeman splitting, i.e., the relative impacts of B_L and the external field B_{dark}, respectively. Note, that B_{dark} does not exceed the so-called mixing field B_m, which was estimated to $\gtrsim$5 mT in Ref. [20], such that Zeemann and spin interaction reservoirs are in lowest order always in thermodynamic equi-

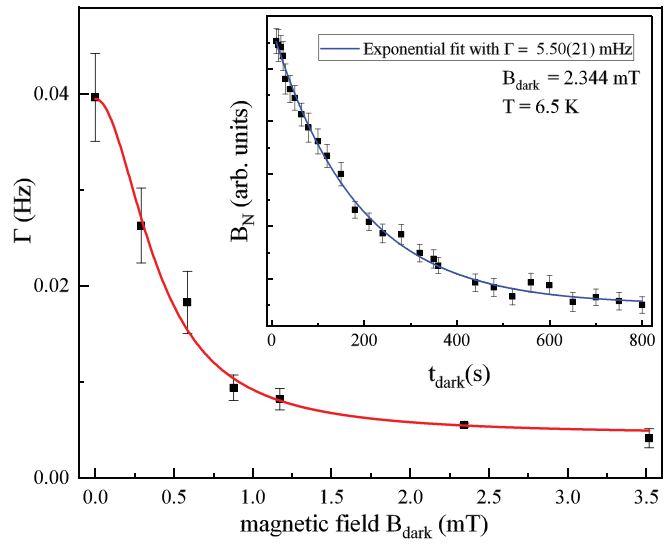

FIG. 1. Measured NSR rate Γ (black squares) as a function of B_{dark} for $n_d = 1.73 \times 10^{16}$ cm^{-3} at $T = 6.5$ *K*. The solid line is a fit to the data according to Eq. (3) with $\xi = 8.79(74)$ and $B_L = 0.39(4)$ mT. Inset: Measured nuclear magnetic field B_N (black squares) in dependence on t_{dark}. The blue line depicts a single exponential fit yielding Γ.

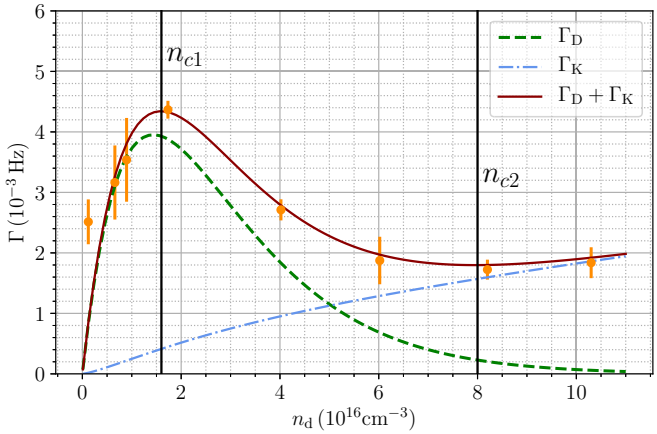

FIG. 2. Dependence of the high field NSR rate Γ, in bulk *n*-type GaAs on doping density measured at $T = 6.5\,K$. Here only the fully delocalized fraction of n_d enters the Korringa rate according to Eq. (2). The values n_{c1} and n_{c2} denote critical densities (see text).

librium [21]. We extract B_L in dependence on doping density for all our samples and find an increase of B_L from 0.35 at $n_d = 1.2 \times 10^{15}$ cm^{-3} to 0.9 at $n_d = 1.03 \times 10^{17}$ cm^{-3} which lies well within previously determined values. In the remaining work, we will focus on the dependency of the extracted $\Gamma = \Gamma_Z$ as the so-called high field ($B_{\mathrm{dark}} \gg B_L$) NSR rate [19] on doping density and sample temperature.

III. DOPING DEPENDENCE OF NUCLEAR SPIN RELAXATION AT HIGH MAGNETIC FIELDS

Figure 2 shows the measured high field NSR rate (orange dots with error bars [22]) in dependence on doping concentration for a lattice temperature of 6.5 K. The two vertical lines denote the critical densities $n_{c1} = 1.6 \times 10^{16}$ cm^{-3} and $n_{c2} = 8 \times 10^{16}$ cm^{-3}, i.e., the point of finite conductivity in the limit of zero temperature MIT and the onset of impurity band hybridization with the conduction band, respectively. At low doping concentrations $n_d < n_{c1}$, Γ increases monotonically with increasing n_d reaching a maximum around n_{c1}. For $n_d > n_{c1}$, Γ decreases in turn with increasing n_d and becomes in good approximation independent of n_d around n_{c2}.

In the following, we want to give a *quantitative* description of this NSR process. The high magnetic field value of Γ is well described by Eq. (1) for very low temperatures and doping concentrations far below the MIT, i.e., $n_d^{-1/3} \gg a_B$. However, the density of localized donors acting as effective drains for the nuclear spin polarization differs significantly for conditions deviating from these constraints. The relative number of fully localized donor electrons decreases with increasing n_d due to the increasing overlap of the donor wave functions, and the original linear increase of Γ_D with increasing n_d in Eq. (1) becomes sublinear. For $n_d > n_{c1}$, not only the relative but even the total number of fully localized donor electrons starts to decrease with increasing n_d. As a consequence, Γ_D decreases and becomes negligible for doping densities above the second MIT (n_{c2}). At the same time, the number of delocalized electrons increases with increasing doping concentration and consequently the NSR rate increases according to the Korringa mechanism described by Eq. (2).

In order to calculate Γ quantitatively, we extract in a first step the fraction of localized electrons η acting as efficient killing centers from the transport measurements on the very same samples presented in Ref. [17] by

$$\eta = 1 - n_H^{6.5\mathrm{K}}/n_d, \tag{4}$$

where $n_H^{6.5\mathrm{K}}$ is the Hall carrier density at 6.5 K and n_d is the doping density extrapolated from the high-temperature Hall measurements. The extracted η can be fitted by

$$\eta = e^{-n_d/\alpha_n}, \tag{5}$$

with $\alpha_n = 1.43(20) \times 10^{16}$ cm^{-3}, whereat the exponential relation between the density of isolated localized donors and n_d results from Poisson statistics. The constant α_n can also be estimated as consistency check by calculating via Poisson statistics the probability of finding a single donor, which wave function—extending over its Bohr radius a_B—does not overlap with other donors (see Appendix C for details concerning the exponential fit and the unpretentious calculation of the probability). Please note that the experimental transport data include already the ionization of the localized donors due to the finite temperature.

In a second step, we calculate (a) the NSR due to diffusion by replacing the total number of donors n_d in Eq. (1) by the number of localized electrons $n_{d,\mathrm{loc}} = \eta\, n_d$ and (b) the NSR rate due to the Korringa mechanism by using $n_H^{6.5\mathrm{K}}$ as the effective number of delocalized electrons. Figure 2 depicts as a green dashed line the resulting NSR due to localized electrons, as a blue dashed-dotted line the NSR due to the Korringa mechanism, and as a solid line the total NSR rate $\Gamma = \Gamma_D + \Gamma_K$. The only adjustable parameter is the average nuclear spin diffusion constant which lies with $D_{\mathrm{av}} = 0.63(6) \times 10^{-13}$ cm^2 s^{-1} [23] in the same range as previously measured values [1]. We want to point out that our measurement is rather precise concerning Γ but not concerning a general value for D_{av}, since (a) the donor electron HF interaction is not a simple hard-sphere killing center for nuclear spins and (b) the values for D differ for the three distinct isotopes for $B \gg B_L$.

IV. TEMPERATURE DEPENDENCE OF THE NUCLEAR SPIN RELAXATION RATE

Figure 2 shows an excellent agreement between experiment and theory for all doping densities but the very lowest one, i.e., $n_d = 1.2 \times 10^{15}$ cm^{-3}. At such a low doping concentration the Korringa mechanism is negligible and the NSR rate due to diffusion to a donor should become significantly lower than experimentally observed. In order to disclose this case, we measure for this low doped sample additionally the temperature dependence of Γ. The orange dots with error bars in Fig. 3 depict Γ in dependence on temperature. The measured Γ first decreases with increasing temperature but starts to increase in turn at higher temperatures. The green dashed line depicts the calculated Γ_D which is significantly too small to explain the experimental data and decreases continuously with temperature due to the thermal ionization of localized electrons [24]. The Korringa mechanism does not play a significant role due to the low carrier density. The experimentally

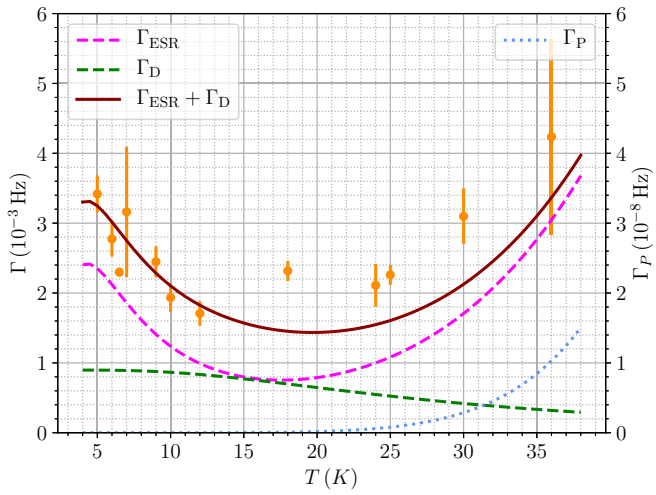

FIG. 3. Temperature dependence of Γ for a doping density of $n_d = 1.2 \times 10^{15}$ cm^{-3} measured at B_{dark}. The NSR due to quadrupolar two-phonon process Γ_P is shown with respect to the right axis. Please note the different scale.

observed increase for $T > 12$ K cannot be attributed to the onset of phonon induced NSR since the impact of dipolar and quadrupolar one- and two-phonon contributions according to calculations is orders of magnitude too small [12]. The highest NSR rate due to phonons Γ_P relies on quadrupolar two-phonon processes and is shown with respect to the right axis in Fig. 3 which differs by five orders of magnitude in comparison to the left axis. Even if these calculations might underestimate Γ_P, comparative measurements from Lu *et al.* [3] on semi-insulating and *n*-doped GaAs confirm that phonon induced NSR can be neglected at low temperatures in *n*-doped GaAs.

One might think that the relatively fast NSR at low temperatures could result from the omnipresent continuous alteration of the local charge environment inducing fluctuating quadrupolar fields which effectively leads to a relaxation of the nuclear spin system into its equilibrium state [25,26]. However, first, the *p*-type background doping is much too small in order to yield a significant density of charged defects and, second, the NSR rate is extracted under dark conditions, i.e., no charge fluctuations due to above band gap excitation can take place. All contributions via spin interaction with delocalized electrons type mechanisms do not play a role here since their magnitude is much too small in this doping regime.

Basically, the only fluctuating source left *radiating* into the nuclear spin bath results from the spin relaxation of the localized donor electrons which has a distinct temperature dependence due to the joint contribution of spin rotation via HF interaction and variable range hopping (VRH). In the simplest case, these fluctuations should contribute an additional NSR rate

$$\Gamma_{ESR} = A_{ESR}\gamma_{s,e}^{(VRH+HF)}, \tag{6}$$

where A_{ESR} is a dimensionless coupling constant and $\gamma_{s,e}^{(VRH+HF)}$ the electron spin relaxation (ESR) rate. The process describes the heat contribution of the localized electron spin dynamics to the nuclear spin system.

Figure 3 shows Γ_{ESR} as a dashed magenta line with $A_{ESR} \cong 6.7 \times 10^{-10}$ being the only fitting parameter. The corresponding electron spin relaxation rate $\gamma_{s,e}^{(VRH+HF)}$ has been calculated according to the values and equations given in Ref. [17] (For more information, see Appendix E). The sum of two calculated rates $\Gamma_{ESR} + \Gamma_D$ yields rather good agreement with the measured NSR. Please note that Γ_{ESR} is implicitly depending on the doping density via the electron spin relaxation rate, which depends on n_d itself. This context has not been included in the calculated density dependence shown in Fig. 2 since (a) the electron spin relaxation rate and its effect of HF interaction and (b) the fraction of localized electrons decreases significantly with increasing doping concentrations.

We want to point out that a quantitative study of this process is beyond the scope of this paper and that the observed correlation between Γ and electron spin relaxation rate is not unambiguous. Molecular beam epitaxy samples with carrier densities of 1.2×10^{15} cm^{-3} and lower have not only a finite carbon background doping concentration but might also have other unintentional side-effects like electric fields and electron depletion or free electrons from under- or overcompensation of the surface Fermi level pinning, respectively.

V. CONCLUSION

In conclusion, we measured the nuclear spin relaxation rate in the high field limit in a contiguous set of accurately characterized *n*-type GaAs samples with different doping densities around the metal-to-insulator transition. The available transport data allows the quantitative calculation of the nuclear spin relaxation rate including only nuclear spin diffusion to the donor electrons as efficient killing centers and Korringa spin relaxation. The calculations yield an excellent agreement between experiment and theory with the spin diffusion constant being the sole adjustable parameter. Only the measured nuclear spin relaxation rate of the very lowest doped sample shows a significant deviation from this quantitative model. Temperature-dependent measurements indicate as cause a nuclear spin heating process by localized electrons with fast HF-induced electron spin relaxation but further experiments and theory are necessary to validate this picture.

ACKNOWLEDGMENTS

We thank J. G. Lonnemann for support concerning the experimental method. This work was funded by the Deutsche Forschungsgemeinschaft (DFG, German Research Foundation) under Germany's Excellence Strategy-EXC-2123 QuantumFrontiers-390837967, research training group 1991, and OE 177/10-2, and the NTH School for Contacts in Nanosystems.

APPENDIX A: MEASUREMENT SETUP AND METHOD

Figure 4 shows the experimental setup for the measurement of the NSR rate using a Hanle-type PL depolarization scheme. Polarization and intensity control of the optical excitation are performed by a half wave plate (λ/2), a linear polarizer (LP), and a quarter wave plate (λ/4). The excitation intensity is always kept so low that the fraction of the optically injected

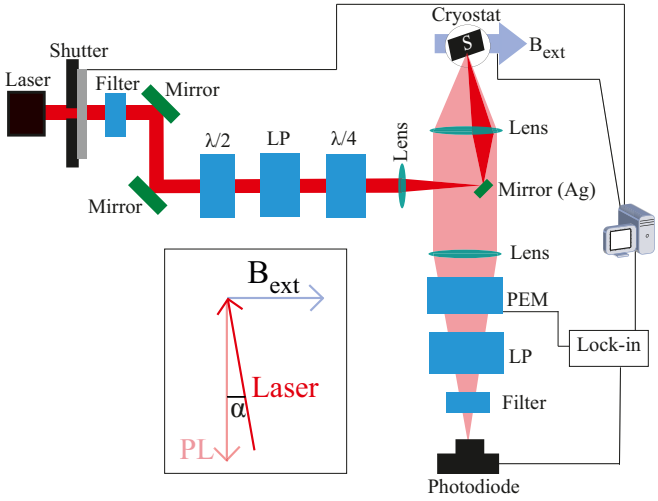

FIG. 4. Schematic representation of the experimental setup for measuring nuclear spin relaxation rates in *n*-type GaAs samples via a Hanle-type depolarization scheme.

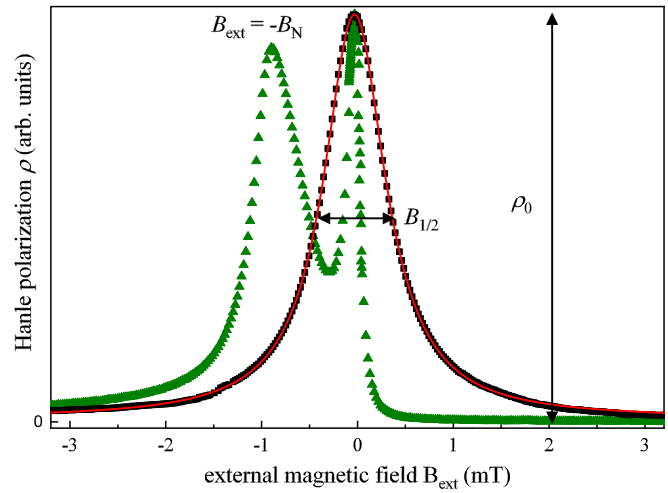

FIG. 5. The black squares depict a typical Hanle curve measured with 50-kHz modulation of the excitation polarization, i.e., without relevant optical pumping of the nuclear spin system, and the red solid line a corresponding Lorentzian fit according to Eq. (A1). The green triangles depict in contrast the measured Hanle curve for excitation with right circularly polarized light where dynamic nuclear spin pumping changes the shape of the Hanle curve drastically [2]. Both Hanle curves are normalized to their respective maxima.

carriers remains at least a factor of hundred below the doping density. An electrically controlled mechanical shutter blocks the laser after 300 s of optical pumping for the time t_{dark} during which the optically pumped nuclear spin system decays exponentially toward its equilibrium state. The Earth's magnetic field is shielded at the sample position by a pair of Helmholtz coils in the direction normal to the applied magnetic field and the detection direction. The degree of circular polarization of the emitted PL is detected in reflection geometry by a Si photodetector and a lock-in amplifier whereat a combination of a 50-kHz photoelastic modulator and a LP is used to alternate the detection between the left (σ_+) and right (σ_-) circularly polarized component of the PL. Spectrally resolved PL measurements confirm in a control experiment that this degree of circular polarization results from the recombination of carriers at the Fermi energy.

Figure 5 shows two preparatory measurements which were carried out for each sample in order to identify the optimal magnetic field for the detection of the nuclear spin polarization. The green triangles are measured with the setup depicted in Fig. 4 by slowly sweeping the amplitude of the external magnetic field and measuring at the same time the degree of PL polarization. The optical pumping by circularly polarized light induces a macroscopic nuclear magnetic field which strongly modifies the shape of the Hanle curve [2]. The black squares show on the other hand a Hanle curve where the polarization components were exchanged between excitation and detection, i.e., the excitation was rapidly modulated between σ_+ and σ_- polarization which efficiently suppresses the build up of nuclear spin polarization. In this case, the Hanle depolarization signal can be very accurately fitted by the Lorentzian function [2]

$$\rho(B) = \frac{\rho_0}{1 + \left(\frac{g\mu_B}{\gamma_e \hbar} B_{\mathrm{eff}}\right)^2}, \tag{A1}$$

where ρ_0 is the Hanle polarization signal at $B = 0$, g is the Landé g factor of the donor bound electron, μ_B is Bohr magneton, and γ_e is the electron spin relaxation rate. The fit is shown as a solid red line in Fig. 5 and its full width at half maximum $B_{1/2} = 2(\frac{\gamma_e \hbar}{g\mu_B})^2$ is a direct measure for γ_e [2]. The two preparatory measurements are necessary in order to choose an external magnetic field for the actual measurement where the change of the PL polarization is large and yields an optimal signal-to-noise ratio.

Figure 6 shows exemplarily Hanle depolarization transients for such an optimal external magnetic field recorded after the process of optical nuclear spin pumping and subsequent NSR in the dark. The amplitude of the PL polarization signal at $t = 0$ s, ρ_{dark}, clearly depends on t_{dark} and decays exponentially due to the repumping of the nuclear spin polarization to its initialization value. The time constant of the exponential decay is approximately constant. The precise amplitude at $t = 0\,s$ is extracted by an exponential fit to these transients and used to calculate the nuclear magnetic fields by [2]

$$B_N = B_{1/2}\sqrt{\frac{\rho_0 - \rho_{\mathrm{dark}}}{\rho_{\mathrm{dark}}}} - B_{\mathrm{pump}}. \tag{A2}$$

The resulting B_N are depicted in the inset of Fig. 1 and can be well fitted by a single exponential decay which yields Γ.

APPENDIX B: LOCAL MAGNETIC FIELD

The local magnetic field B_L is directly extracted with Eq. (3) from the measurements of Γ versus B_{dark} as exemplified in Fig. 1. The inset of Fig. 6 depicts the resulting B_L as blue squares with error bars and for comparison literature values which show on the whole a comparable increase with n_d, which reason, however, is open. Please note that the literature values are not measured on a contiguous set of samples but with varying methods on differing GaAs bulk and microcavity

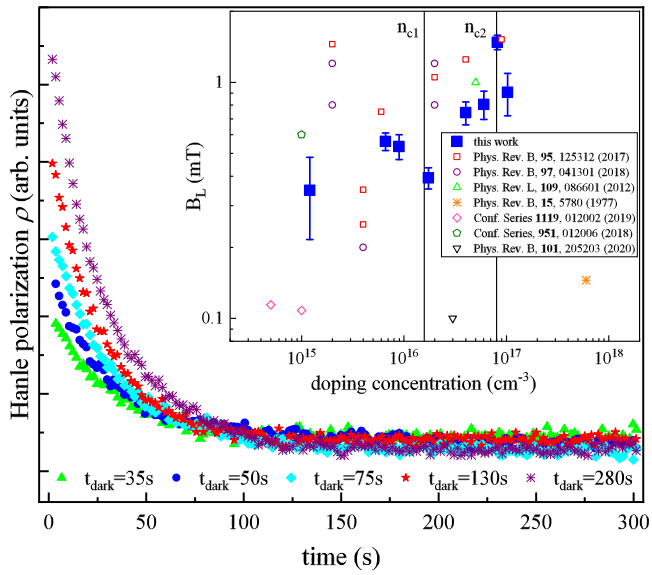

FIG. 6. Hanle depolarization transients recorded after different dark times for $n_d = 6.02 \times 10^{16}$ cm^{-3}, $B_{\rm dark} = 1.17$ mT, and T = 6.5 K. The opening of the laser shutter defines $t = 0$ s. The inset shows the density dependence of the local magnetic field which has been extracted from the measured $\Gamma(B_{\rm dark})$ according to Eq. (4) (blue squares). The other symbols depict for comparison a compilation of B_L from literature.

samples where for example varying strain-induced quadrupole splittings lead to a significant scattering of the measured B_L [14,16,20,27–30].

APPENDIX C: SAMPLES AND DEGREE OF LOCALIZATION

Table I summarizes the sample properties extracted from transport measurements while the black squares in Fig. 7 show

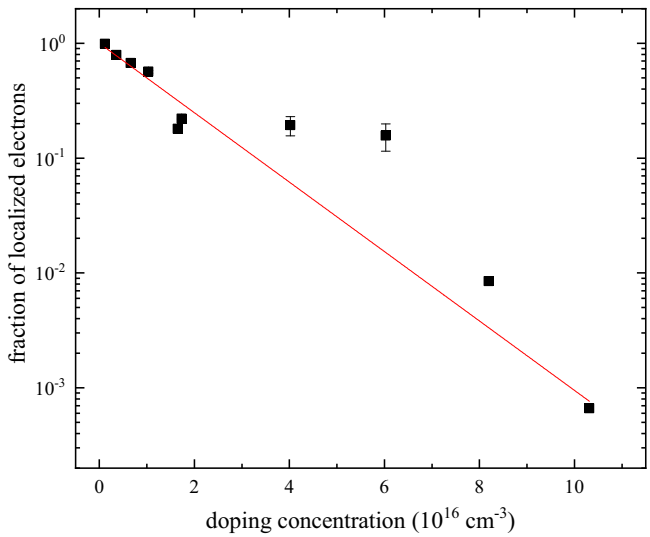

FIG. 7. Dependence of the localization fraction η on doping density.

the dependence of the localization fraction η on the doping density n_d. The localization fraction has been calculated with Eq. (4) and $n_H^{6.5\rm K}$ from Ref. [17]. The red line in Fig. 7 is a fit to e^{n_d/α_n} with $\alpha_n = 1.43(20) \times 10^{16}$ cm^{-3}. Such an exponential relation between the number of isolated single donors and n_d follows directly from Poisson statistics. A finite deviation of η calculated from the measured $n_H^{6.5\rm K}$ with Eq. (4) is not surprising for $n_d > n_{\rm c1}$ since not only the localization of single donor electrons but also the localization of ensembles of donor electrons start to play a role. In contrast to single localized electrons such localized ensembles of interacting electrons are not as efficient nuclear spin "killing centers."

The constant α_n can also be estimated via Poisson statistics from the probability of finding a single donor which wave function—extending over its Bohr radius a_B—is nonoverlapping with other donors, i.e., which is noninteracting apart from screening effects, and can count as active magnetic impurity. With $\mu = n_d/n_\ell$, where n_ℓ is the lattice site density of the host crystal, the probability that a site is not occupied by a donor is $e^{-\mu}$. The exclusive volume where no other donor overlap exists is $V_{\rm no} = \frac{4\pi}{3}(2a_B)^3$. The total probability $p(n_d)$ of finding such a situation is given with $N_{\rm no} = V_{\rm no} n_\ell$ as

$$p(n_d) = \prod_{i=1}^{N_{\rm no}} e^{-\mu} = e^{-\frac{32}{3}\pi a_B^3 n_d}. \tag{C1}$$

The prefactor in the exponent in Eq. (C1) equals the experimentally determined α_n for an effective Bohr radius of $a_B^{\rm eff} \approx 12.8$ nm which is only slightly larger than the typical donor Bohr radius for Si dopants in GaAs. Such a slightly larger radius is not unexpected since the donor electron wave function extends beyond a_B. Also, screening and any other interaction effects have not been considered in this basic estimate.

APPENDIX D: CARRIER STATISTICS

The number of localized carriers reduces with increasing temperature due to ionization. This effect is included in our calculations by Blakemore's equation for the temperature dependence of the number of localized donor electrons [24],

$$n_{d,\rm loc}(T) = n_d - \frac{2n_d}{1 + \sqrt{1 + 4\beta n_d / n_{\rm cb,eff} e^{E_d/(k_B T)}}}, \tag{D1}$$

where $E_d = 5.8$ meV is the donor binding energy, β is the spin degeneracy of the donor state, $n_{\rm cb,eff} = 2(2m_e^\star k_B T)^{3/2} h^{-3}$ is the effective density of states, and $m_e^\star = 0.067 m_0$ is the effective electron mass in GaAs.

APPENDIX E: ELECTRON SPIN RELAXATION RATE

The electron spin relaxation rate in Eq. (6) includes VRH and HF spin relaxation rates, i.e., $\gamma_{s,e} = \gamma_{\rm VRH} + \gamma_{\rm HF}$. The following is a short summary of the calculations presented in Ref. [17]. The VRH spin relaxation rate for electrons hopping between two impurities separated by R_{ij} with a rate of $\tau_{\rm hop}^{-1}$ is given by:

$$\gamma_{\rm VRH} = \tau_{s,\rm hop}^{-1} = \frac{2}{3}\langle\theta^2(R_{ij})\rangle/\tau_{\rm hop}. \tag{E1}$$

Here the electron spin rotates by a small rotation angle $\theta(R_{ij})$ during each hop due to spin orbit interaction entailing an effective relaxation of the spin polarization. The hopping time $\tau_{\rm hop} = D_{\rm hop}/(6R_{\rm opt}^2)$ is defined by (a) the specific diffusion constant $D_{\rm hop} = \mu_H \frac{k_B T}{e_0} = \frac{\sigma_{\rm hop} k_B T}{n_H e_0^2}$ with the Hall mobility μ_H and (b) the optimal hopping distance $R_{\rm opt} = [9a_d/(8\pi N_{E_F} k_B T)]^{1/4}$. The effective Hall carrier density n_H is the difference between the impurity and conduction band carrier densities $n_{\rm di}$ and $n_{\rm cb}$, respectively. The optimal hopping distance depends on the density of states at the Fermi energy N_{E_F}, which is the only free parameter available from the temperature dependence of the measured conductivity (see Fig. 4 from Ref. [17]):

$$\sigma_{\rm hop}(T) = \sigma_0(N_{E_F}) T^{-1/2} e^{-[T_0(N_{E_F})/T]^{1/4}}, \tag{E2}$$

where $T_0 = 512/(9\pi a_B^3 k_B N_{E_F})$ and $\sigma_0 T^{-1/2} = e^2 R_{\rm opt}^2 \nu_H N_{E_F}/6$ are used with the attempt rate given by the phonon frequency $\nu_H = 8.8$ THz [31]. We use the relation from Gor'kov and Krotkov [32] for calculating $\langle\theta^2(R_{ij})\rangle$.

The relaxation rate from the HF interaction is calculated via Eq. (7) from Ref. [17]:

$$\gamma_{\rm HF} = \tau_{s,\rm HF}^{-1} = \langle\Omega_N^2\rangle\tau_c = (\mu_B g^*/\hbar)^2\langle B_N^2\rangle\tau_c, \tag{E3}$$

with $\tau_c = \tau_{\rm hop}$, $B_N = 5.4$ mT, and the energy-dependent effective electron g factor [33].

[1] D. Paget, Phys. Rev. B **25**, 4444 (1982).
[2] F. Meier and B. P. Zakharchenya, eds., *Optical Orientation* (North-Holland, Amsterdam, 1984).
[3] J. Lu, M. J. R. Hoch, P. L. Kuhns, W. G. Moulton, Z. Gan, and A. P. Reyes, Phys. Rev. B **74**, 125208 (2006).
[4] J. Huang, Y. S. Chen, A. Ludwig, D. Reuter, A. D. Wieck, and G. Bacher, Appl. Phys. Lett. **100**, 132103 (2012).
[5] R. Giri, S. Cronenberger, M. M. Glazov, K. V. Kavokin, A. Lemaître, J. Bloch, M. Vladimirova, and D. Scalbert, Phys. Rev. Lett. **111**, 087603 (2013).
[6] M. Kotur, R. I. Dzhioev, M. Vladimirova, B. Jouault, V. L. Korenev, and K. V. Kavokin, Phys. Rev. B **94**, 081201(R) (2016).
[7] M. I. Dyakonov, ed., *Spin Physics in Semiconductors*, 2nd ed., Springer Series in Solid-State Sciences, Vol. 157 (Springer, Cham, 2017).
[8] M. M. Glazov, *Electron and Nuclear Spin Dynamics in Semiconductor Nanostructures*, 1st ed., Series on Semiconductor Science and Technology, Vol. 23 (Oxford University Press, Oxford, 2018).
[9] P. S. Sokolov, M. Y. Petrov, K. V. Kavokin, M. S. Kuznetsova, S. Y. Verbin, I. Y. Gerlovin, D. R. Yakovlev, and M. Bayer, Phys. Rev. B **99**, 075307 (2019).
[10] P.-G. de Gennes, J. Phys. Chem. Solids **7**, 345 (1958).
[11] J. Korringa, Physica **16**, 601 (1950).
[12] A. Abragam, *The Principles of Nuclear Magnetism*, reprinted ed., Int. Ser. of Monographs on Physics, Vol. 32 (Oxford University Press, Oxford, 1961).
[13] G. Kaur and G. Denninger, Appl. Magn. Reson. **39**, 185 (2010).
[14] D. Kölbl, D. M. Zumbühl, A. Fuhrer, G. Salis, and S. F. Alvarado, Phys. Rev. Lett. **109**, 086601 (2012).
[15] M. Kotur, R. I. Dzhioev, K. V. Kavokin, V. L. Korenev, B. R. Namozov, P. E. Pak, and Y. G. Kusrayev, J. Exp. Theor. Phys. Lett. **99**, 37 (2014).
[16] M. Vladimirova, S. Cronenberger, D. Scalbert, M. Kotur, R. I. Dzhioev, I. I. Ryzhov, G. G. Kozlov, V. S. Zapasskii, A. Lemaître, and K. V. Kavokin, Phys. Rev. B **95**, 125312 (2017).
[17] J. G. Lonnemann, E. P. Rugeramigabo, M. Oestreich, and J. Hübner, Phys. Rev. B **96**, 045201 (2017).
[18] The error bars in this publication are the measured statistical errors only and do not include potential systematic errors.
[19] M. Goldman, *Spin Temperature and Nuclear Magnetic Resonance in Solids*, The International Series of Monographs on Physics (Clarendon Press, Oxford, 1970).
[20] M. Vladimirova, S. Cronenberger, D. Scalbert, I. I. Ryzhov, V. S. Zapasskii, G. G. Kozlov, A. Lemaître, and K. V. Kavokin, Phys. Rev. B **97**, 041301(R) (2018).
[21] The value for ξ in our measurements is on average larger than the maximal theoretical estimated limit of 2 to 3 given in Ref. [19] for low magnetic fields. This could be also attributed to additional relaxation mechanisms contributing to Γ_{ss} at zero external fields, as pointed out, e.g., in Ref. [6] .
[22] The error bars of Γ are extracted from exponential fits of $B_{\rm N}$ versus $t_{\rm dark}$ which is exemplarily shown for $n_{\rm d} = 1.73 \times 10^{16}{\rm cm}^{-3}$ in the inset of Fig. 1. Here, the error bars of $B_{\rm N}$ are extracted from the exponential fits of the PL polarization versus laboratory time.
[23] We use $a_{\rm B} = 10.1$nm.
[24] J. S. Blakemore, *Semiconductor Statistics* (Dover, Mineola, NY, 2002).
[25] D. Paget, T. Amand, and J.-P. Korb, Phys. Rev. B **77**, 245201 (2008).
[26] M. Kotur, R. I. Dzhioev, M. Vladimirova, R. V. Cherbunin, P. S. Sokolov, D. R. Yakovlev, M. Bayer, D. Suter, and K. V. Kavokin, Phys. Rev. B **97**, 165206 (2018).
[27] D. Paget, G. Lampel, B. Sapoval, and V. I. Safarov, Phys. Rev. B **15**, 5780 (1977).
[28] V. M. Litvyak, R. V. Cherbunin, K. V. Kavokin, and V. K. Kalevich, J. Phys.: Conf. Ser. **951**, 012006 (2018).
[29] A. E. Evdokimov, M. S. Kuznetsova, M. Y. Petrov, R. A. Potekhin, Y. P. Efimov, S. A. Eliseev, V. A. Lovtcius, and P. Y. Shapochkin, J. Phys.: Conf. Ser. **1199**, 012002 (2019).
[30] M. J. Dominguez, J. R. Iafrate, and V. Sih, Phys. Rev. B **101**, 205203 (2020).
[31] C. Patel, T. Parker, H. Jamshidi, and W. Sherman, Phys. Status Solidi B **122**, 461 (1984).
[32] L. P. Gor'kov and P. L. Krotkov, Phys. Rev. B **67**, 033203 (2003).
[33] J. Hübner, S. Döhrmann, D. Hägele, and M. Oestreich, Phys. Rev. B **79**, 193307 (2009).